NIH Public Access
Author Manuscript
Nanoscale. Author manuscript; available in PMC 2014 December 07.

Published in final edited form as:
Nanoscale. 2013 December 7; 5(23): 11394–11399. doi:10.1039/c3nr02203j.

Cytotoxicity and DNA cleavage with core-shell nanocomposites functionalized by a KH domain DNA binding peptide

Remon Bazak[a,b], **Jan Ressl**[b], **Sumita Raha**[b], **Caroline Doty**[b], **William Liu**[b], **Beau Wanzer**[b], **Seddik Abdel Salam**[a], **Samy Elwany**[a], **Tatjana Paunesku**[b], and **Gayle E Woloschak**[b]

Remon Bazak: dr_remon77@yahoo.com; Gayle E Woloschak: g-woloschak@northwestern.edu

[a]Department of Otorhinolaryngology and Head & Neck Surgery, University of Alexandria Medical School, Azarita medical campus, Champlollion Street, Khartoum Square, Alexandria, Egypt. Tel: 01003810548

[b]Departments of Radiation Oncology and Radiology, Northwestern University Feinberg School of Medicine, 303 East Chicago Avenue, Chicago, Illinois 60611 USA. Fax: 312-577-0751; Tel: 312-503-4322

Abstract

A nanoconjugate was composed of metal oxide nanoparticles decorated with peptides and fluorescent dye and tested for DNA cleavage following UV light activation. The peptide design was based on a DNA binding domain, the so called KH domain of the hnRNPK protein. This “KH peptide” enabled cellular uptake of nanoconjugates and their entry into cell nuclei. The control nanoconjugate carried no peptide; it consisted only of the metal oxide nanoparticle prepared an Fe3O4@TiO2 nanocomposite and the fluorescent dye alizarin red S. These components of either construct are responsible for nanoconjugate activation by UV light and the resultant production of reactive oxygen species (ROS). Production of ROS at different subcellular locations causes damage to different components of cells: only nanoconjugates inside cell nuclei can be expected to cause DNA cleavage. Degradation of cellular DNA with KH peptide decorated nanoconjugates exceeded the DNA damage obtained from control, no-peptide nanoconjugate counterparts. Moreover, caspase activation and cell death were more extensive in the same cells.

Introduction

Small molecule anti-cancer therapeutics generally kill malignant cells with high efficacy but little precision.[1, 2] By comparison, the use of nanoparticles allows greater flexibility for developing targeting strategies; predominantly because surfaces of most nanoparticles offer an ample area for nanoparticle functionalization.[3]

While active targeting often means that the nanoparticle recognizes a specific target on the surface of the malignant cell,[4] the specificity of a nanoparticle’s anti-cancer activity can also be amplified by designing the nanoparticles with intracellular targeting capability. This is

Correspondence to: Remon Bazak, dr_remon77@yahoo.com; Gayle E Woloschak, g-woloschak@northwestern.edu.

†Electronic Supplementary Information (ESI) available: http://janus.northwestern.edu/wololab/auxiliary/supplementary_data_2013.docx See DOI: 10.1039/b000000x/

NIH-PA Author Manuscript
NIH-PA Author Manuscript
NIH-PA Author Manuscript

NIH-PA Author Manuscript

NIH-PA Author Manuscript

NIH-PA Author Manuscript

especially true for nanomaterials with a trigger-dependent cytotoxic modality such as light activation. Semiconductor nanomaterials based on titanium dioxide (TiO_2) fall into this category because when activated they oxidize nearby molecules directly or through the action of reactive oxygen species (ROS) that are produced upon interactions with water molecules.[5, 6] However, due to their short lifetime in aqueous solution, the diffusion distance of TiO_2 produced hydroxyl radicals (3OH) in pure water is at most 1.1 micron which means that these nanoparticles would be the most efficient DNA damaging agents if they were present inside the cell nucleus.[5, 6] Therefore, DNA-specific intracellular delivery of TiO_2 nanoparticles is a necessary prerequisite for highly targeted damage of DNA. This exact mode of use of TiO_2 nanoparticles has not been utilized so far. Most research on TiO_2 nanoparticle light induced cytotoxicity involves cell membrane targeting of the nanoparticles, if any, coupled with exposure to large doses of illumination which at its own can cause significant cell death.[7] Light activation of membrane targeted or non-targeted TiO_2 nanoparticles has been used to initiate cell death, but the proposed mechanism of cytotoxicity was lipid peroxidation.[8–10] Any DNA damage in such cells was a result of apoptotic processes rather than direct damage to the DNA itself.[11]

In this work we present a new DNA targeting strategy for nanoparticles which facilitates tethering of the nanoparticles in close proximity to genomic DNA. Nanoconjugates were prepared using a platform of photoreactive nanocomposites conjugated to a peptide having DNA targeting capability. These nanoconjugates were investigated for their capacity to cleave plasmid DNA *in vitro* and genomic DNA in cells (Figure 1).

Results and discussion

Photoreactive nanocomposites were prepared as core-shell nanocomposites, with a 3.1 nm Fe_3O_4 core covered with a TiO_2 shell, for the final nanoparticle size averaging at about 6.5 nm (supplemental data).[12] Doping TiO_2 with Fe_3O_4 makes the whole construct more susceptible to light excitation[8, 13] and at the same time compatible with magnetic resonance imaging thus increasing its potential applications. In order to facilitate visualization of these nanocomposites, 23% of the nanocomposite surface was covered with Alizarin red S (ARS) which binds well with TiO_2 surfaces and renders the particles visible by optical fluorescence.[14] The KH peptide (AGAVIGKGG) derived from the protein hnRNPK which is responsible for binding of this protein to nucleic acids[15, 16] was used for nanocomposite surface functionalization. hnRNPK is one from the series of proteins that bind both poly-C DNA sequences and RNA molecules.[16] These proteins regulate varied cellular processes dependent on nucleic acids, causing up and down regulation of both transcription and translation.[15, 16] The short peptide we selected corresponds to the amino acids 54 through 72 from the central part of the KH1 domain and includes the end of the alpha 1 helix and the GXXG loop which is critical for interaction with the nucleic acids. The complete KH domain (KH1 domain spans amino acids 42 to 104) typically recognizes only four nucleotides; its complete binding cleft contains alpha 1-helix, GXXG loop, alpha 2-helix, beta 2-strand, and a variable loop.[17]

Several experiments were undertaken to evaluate the ability of the KH peptide to facilitate interactions between the nanocomposite they decorate and exogenous DNA. In one of the

NIH-PA Author Manuscript NIH-PA Author Manuscript NIH-PA Author Manuscript

preliminary experiments, a 2 kb long coding sequence of the myc gene sequence was denatured and conjugated to the nanoparticles bearing on the surface both KH peptide and ARS. These hybrid DNA probes-nanoparticles were then tested as probes for fluorescent in situ hybridization (FISH) (Supplemental Figure 4). While FISH generally requires long DNA sequences as probes, in this instance hybridization of a relatively short DNA segment was stabilized by the presence of the KH peptide, while ARS labeling of the nanoparticle allowed screening of hybridization events (Supplemental Figure 4). This facilitation of DNA hybridization by the presence of a KH peptide may be a result of the fact that KH peptide mimics the protein hnRNPK (of which it is a part) which binds to the promoter of the myc gene.[17]

To test the ability of KH peptide to act at its own as a DNA binding anchor for nanoparticles, we mixed the KH peptide decorated nanocomposites with the double-stranded supercoiled plasmid carrying a 7 kb insert with the complete genomic sequence of human papilloma virus 18 (HPV18) *in vitro* and then exposed it to light. The difference in plasmid DNA degradation in the absence or presence of nanocomposites was most notable with nanocomposites conjugated with KH peptide. Figure 2 shows the results of the *in vitro* cleavage experiment. Lanes 7 and 8, with the nanoparticles decorated with KH peptide, show the greatest difference in quantities of supercoiled DNA (black arrow) and nicked, partially degraded DNA (white arrow) before (lane 8) and after (lane 7) activation of nanoparticles by illumination.

This plasmid DNA sequence is a native target for the papilloma virus' transcription factor E2 which also uses a KH-like motif for DNA binding.[18] In addition, this complex sequence carries several sites with five or more cytosines in a row, which is a conservative putative sequence of hnRNPK protein. Binding of either hnRNPK or E2 to nucleic acids is similarly promiscuous; for example, E2 protein is known to interact not only with its putative 1,094 DNA matches in the host genome, but with an additional 2,294 sites, many of them in the active chromatin regions.[18] The KH peptide resemble the properties of the complete KH domain from the hnRNPK protein, however, small peptide size makes it possible to attach several copies of the peptide to each nanoparticle and increase nanoconstruct's affinity for DNA even though the peptide sequence is of short length. Due to the short length and the relative sequence recognition promiscuity of this type of DNA binding peptides, the nanoparticles decorated by KH peptide interacted with complex DNA targets on numerous sites which resulted in tethering of the nanocomposites close to the DNA molecule. Photoexcitation of nanocomposites and subsequent production of ROS caused DNA cleavage more efficiently than when the particles were free in suspension.

Once the DNA breakage-inducing behavior of the KH carrying nanocomposites was demonstrated with pure DNA, we applied the same nanoconjugates to cells in culture to obtain a more functional proof. The nasal cancer cell line RPMI 2650 was treated with the nanoparticle constructs for a period of one hour, then illuminated with ultraviolet (UV) light for 10 min, fixed and the immunofluorescence was done for 53BP1 protein as an indicator of double-stranded DNA breaks in cell nuclei.[19] Figure 3 presents the results of these experiments; a diffuse staining for 53BP1 with occasional foci in the nucleus predominated in all of the cells that were not UV illuminated. Of the illuminated cells, those that were not

NIH-PA Author Manuscript

NIH-PA Author Manuscript

NIH-PA Author Manuscript

treated with particles preserved the same diffuse appearance, while all cells treated by nanocomposites showed the presence of 53BP1 foci which indicate sites of DNA breaks. However, some of the cells treated with the nanocomposites functionalized by KH peptide were observed to have nuclei almost devoid of 53BP1 staining and with densely stained pyknotic nuclei (arrows) suggesting onset of apoptosis. For more details see supplemental data.

To investigate the apoptotic behavior of cells treated with KH peptide nanocomposites, we repeated the same experimental conditions but stained the cells for caspase-cleaved-CK18 cytokeratin using the antibody M30.[20] Again, all the cells that were incubated with the KH peptide nanoparticles demonstrated a cytoplasmic as well as nuclear distribution of the nanoparticles. However, M30 staining, suggesting early apoptosis, was found only in cells carrying KH peptide nanoparticles after illumination with UV (Figure 4). Some of these cells also had decreased cell volume, nuclear condensation and nuclear fragmentation, all of which are features of apoptosis. For more details see supplemental data.

It is noteworthy that nanoparticles coated only with ARS enter cells through all possible endocytotic mechanisms, arriving eventually into the cytoplasm but not the nucleus.[14] On the other hand, the KH peptide surface coating renders the nanoparticles capable of entering the nucleus (Figures 3 and 4). While other peptides that improve cellular uptake have been developed,[21] KH peptide served a dual function; firstly it improved cellular as well as nuclear uptake and then it promoted co-localization of the nanoparticles with the genomic DNA. Excitation of nanocomposites under these circumstances caused frequent DNA double strand breaks, occasionally even degrading much of the cellular DNA (Figure 3) with subsequent cell death.

By virtue its low sequence specificity, this peptide confers onto nanoparticles an ability to interact with multiple sites on DNA. Consequently, ROS production following light activation of these nanocomposites causes DNA cleavage in cells at multiple DNA sites even at low nanoparticle concentrations (25 mg/L of TiO_2 and 14 mg/L of Fe) and low (0.5 J/cm2) doses of UVB light.

To obtain statistics for cell death events caused by activation of KH-peptide functionalized, ARS conjugated-nanocomposites, we conducted flow cytometric cell death analysis. Cells were exposed to nanocomposites for 1 h, half of them were exposed to UV light for 10 min and cell death was evaluated by flow cytometry 24 h later. In this experiment (Figure 5) drop in the number of viable cells and the formation of cell debris were most pronounced in the cells treated with the KH functionalized ARS coated nanocomposites and exposed to UV light. A less pronounced decrease of viable cell number was found in cells treated with nanocomposites coated with ARS alone. These nanocomposites accumulated in cell nuclei much less than their KH peptide functionalized counterparts (see Figures 3 and 4). For additional details see supplemental material (Supplemental Figure 5).

It is important to note that many nanoparticle types show inherent or inducible cytotoxicity. For example, ultrafine iron oxide nanoparticles with citrate coating, similar to the core particles of the core-shell nanocomposites under discussion here, are cytotoxic at iron

NIH-PA Author Manuscript

NIH-PA Author Manuscript

NIH-PA Author Manuscript

concentrations above 500 mg/L.[22] In these experiments, however, iron concentrations in cell media never exceeded 14 mg/L, moreover, surface modifications of iron oxide nanoparticles were found to be critical for majority of cytotoxicity effects;[22] while in this case iron oxide was encased in a TiO_2 shell. A recent overview of TiO_2 nanoparticles and their cytotoxicity when photoactivated indicated that TiO_2 cytotoxicity entirely depends on illumination,[7] which was at a substantially higher dose (5.4 to 7.5 J/cm^2) than used in the experiments presented here. However, since there is no direct match between nanoparticle sizes and types and the wavelength of UV light used, it is difficult to make direct comparisons between the work of Sanders and others[7] and the work presented here. In our work we observed marked differences between samples treated by non-targeted nanocomposites and the nanocomposites functionalized by KH peptide only after photoactivation by a 0.5 J/cm^2 UVB exposure.

In summary, incubation of malignant nasal cells with photoexcitable KH-nanocomposites followed by exposure to UV light resulted in DNA cleavage *in vitro* and pronounced apoptosis compared to control cells. This can be attributed to the functionalization with KH peptide which promoted nuclear translocation of the nanocomposites and increased their proximity to genomic DNA thereby facilitating the ROS induced DNA damage.

Experimental

Preparation of surface functionalized iron oxide core-titanium dioxide shell nanocomposites

Nanocomposites described in Arora et al.[12] were used for these experiments. Briefly, 3.1 nm Fe_3O_4 nanoparticles, as measured by Atomic Force Microscopy (AFM), that later served as particle cores were prepared in aqueous solution from ferro and ferric chlorides in the presence of citric acid. The mixture was stirred for 3 h at room temperature then incubated at 65°C over night. Chilled 0.09 M titanium tetrachloride solution was added drop-wise to the diluted, chilled and filtered Fe_3O_4 nanoparticle suspension. The colloidal mixture was stirred for 6 h and stored at 4 °C. The concentration of the core-shell nanoparticles was determined by Inductively Coupled Plasma Mass Spectrometry (ICP-MS) following removal of excess molecular Ti and Fe chlorides by dialysis. The size and size distribution of final core-shell nanocomposites were examined by atomic force microscopy. The size of Fe_3O_4@TiO_2 core-shell nanoparticles averaged around 6.5 nm in diameter by AFM. Based on concentration of Ti and nanoparticle size, the stock nanoparticle concentration was calculated to be 83 nM (with 280 mg/L of TiO_2 and 150 mg/L of Fe).12 All chemicals were purchased from Sigma. The capacity of non-functionalized nanoparticles to cause DNA cleavage *in vitro* was tested with a “plasmid DNA breakage” assay (Supplemental Figure 1).

Titanium atoms on surfaces of nanoparticles smaller than 20 nm are five-coordinated and readily bind catechols and catechol conjugated ligands which repair such corner defects.[23] Previously, we have used dopamine to attach oligonucleotides to TiO_2 nanoparticles.14, 24 Inside cells, such nucleic acid carrying nanocomposites demonstrated extended retention in specific subcellular locations.[25]

NIH-PA Author Manuscript

NIH-PA Author Manuscript

NIH-PA Author Manuscript

Prior to surface functionalization, aliquots of core-shell nanocomposites were neutralized by rapid addition of 10 M NaOH to a pH = 4. The KH peptide [N-terminus] dopamine-AGAVIGKGG [C terminus] was synthesized with dopamine on its N terminal end and purified to 85% (PrimmBiotech, Inc.). Its sequence was derived from the hnRNPK protein sequence (UniProt ID P61978), amino acids 54–72. This sequence is a part of the KH1 domain which spans over amino acids 42 to 104 and is responsible for binding of hnRNPK to nucleic acids.[15] The conjugation between the nanoparticles and the KH peptide was confirmed by UV-visible light spectroscopy using the NanoDrop ND-1000 Spectrophotometer (Supplemental Figure 2).

Subsequently, Alizarin red S (ARS) was also coupled to the nanocomposite surface. The conjugation between ARS and TiO_2 surfaces smaller than 20 nm is efficient and has been shown to remain stable inside cells.[14, 26] We used ARS coating to make the nanoparticles fluorescent, in order to be able to follow their distribution in cells by microscopy and flow cytometry as we have done previously.[14] Based on the average radius and calculated surface area, about 23% of the nanoparticle surface was coated with ARS while an additional 11% was covered by the KH peptide; each conjugation step was done in oxygen free atmosphere over night.

Dynamic light scattering (DLS) was used to determine the zeta potentials of the bare nanoparticles, ARS coated nanoparticles, and KH-peptide-ARS coated nanoparticles (Supplemental Figure 3). Samples for DLS analysis were diluted 1:100 in distilled water and injected into clear disposable capillary tubes (Malvern DTS1061). The zeta potentials were read in triplicate on a Malvern Zetasizer Nano. The zeta potentials of different samples were close to −35 in all cases (Supplemental Figure 3).

Plasmid DNA

Plasmid pGEMII-WT with the entire 7.9 kb genome of human papilloma virus 18 inserted into the EcoRI restriction site at nucleotide 2440 of plasmid pGEMII was a gift from L. Lamins from Northwestern University, and was originally generated by Stubenrauch laboratory.[27] Plasmid was grown in *E. coli* and harvested according to manufacturers' instructions using a standard midi prep Qiagen kit.

Plasmid DNA breakage assay

DNA breakage of supercoiled plasmid into relaxed (nicked) plasmid form is a standard assay used frequently to asses ROS production *in vitro*.[28] Plasmid DNA was suspended in 10 mM sodium phosphate buffer pH = 6 and mixed with "bare" nanocomposites, ARS coated, or ARS and KH peptide functionalized nanocomposites. Following an incubation of 30 min at 37°C, samples were transferred onto ice. In all cases, the final nanocomposite concentration was 100 nM (or 46 mg/L concentration of TiO_2 and 25 mg/L of Fe). One half of each mixture was illuminated for 10 min at maximum intensity with a quartz halogen lamp (Fiber Lite MI-150, Dolan Jenner) prior to loading on a 1% agarose gel (SeaKem LE agarose, Lonza). Samples were subjected to electrophoresis in Tris-acetate-EDTA buffer for 13 h at 40 V and the gel stained with Gel Star (Cambrex).

NIH-PA Author Manuscript NIH-PA Author Manuscript NIH-PA Author Manuscript

Cell culture and nanoparticle treatments

A squamous cell carcinoma cell line isolated from nasal septum RPMI 2650[29] was obtained from ATCC and grown in ATCC formulated Eagle's Minimum Essential Medium, with fetal bovine serum at a final concentration of 10% supplemented with antibiotics in a humidified 5% CO_2 atmosphere at 37°C.

In order to ensure that DNA double strand break foci were sites of DNA breaks and not created in the course of DNA synthesis, we routinely synchronized the RPMI 2650 cells in M phase of cell cycle by a mitotic shake-off. Harvested cells were allowed to re-enter G1 phase of the cell cycle; complete cell cycle of this cell line lasts approximately 30–32 h. The RPMI 2650 cells were treated with nanocomposites and illuminated during the G1 phase of the cell cycle. Cells for microscopy were grown on glass slides and exposed to 60 nM nanoparticles (or 25 mg/L TiO_2 and 14 mg/L Fe) coated either with ARS only (12 μM) or in combination with KH peptide (6 μM) for 1 h, applied 12 h after plating. Both control and nanocomposite treatments were done in 500 μL of complete media. Treated and control slides were washed with phosphate buffered saline (PBS), then exposed to a 254 nm UV bench lamp (~0.5 J/cm^2) under a thin layer of PBS with calcium and magnesium. After illumination, the slides were again submerged in full media and returned to cell incubator for 30 min. Acid glycine wash (0.2 M glycine and 0.15 NaCl, pH=3) was done immediately before the cells were fixed in 3.6% formaldehyde.

Immunocytofluorescence

53BP1—Following a 10 min fixation cells were washed with PBS and permeablized in PBS-Triton 100x (0.2%) for 10 min. Following a series of washes in PBS with 1% bovine serum albumin (BSA) and 0.1% Tween, cells were incubated with primary Rabbit anti-53BP1 antibody (Abcam) in dilution of 1:200 in PBS-BSA 1% – Tween 0.1% at room temperature for 60 min. Slides were washed, incubated with the secondary antibody (Alexa Fluor® 488 goat anti-rabbit IgG, Abcam) at 400 fold dilution for 45 min, washed again and the nuclei were counterstained with 1:50000 diluted Hoechst 33342 (Invitrogen) for 10 min at room temperature. Finally, slides were washed with PBS and mounted with ProLong Gold antifade reagent (Invitrogen) and imaged with Nikon C1si confocal microscope at Northwestern Cell Imaging Facility.

M30—Treatment and staining for apoptosis evaluation differed by the length of incubation post-illumination (24 h instead of 30 min); primary antibody was M30 (Roche) which detects a cleaved form of cytokeratin 18. This primary antibody was used diluted at 1:50 ratio; secondary antibody and wash steps were the same as for 53BP1.

Flow cytometry analysis of apoptosis and necrosis

Control cells and cells treated with different formulations of nanoparticles were sham illuminated or illuminated with UV light as described above. For each treatment, about 10^5 cells were collected by trypsinization. Cells were centrifuged and resuspended in annexin-binding buffer (10 mM HEPES, 140 mM NaCl, and 2.5 mM $CaCl_2$, pH = 7.4) and stained according to the manufacturer's instructions. Staining was done with 5 μL allophycocyanin (APC) annexin V conjugate (Invitrogen) per 100 μL sample; staining with SYTOX Blue

NIH-PA Author Manuscript

NIH-PA Author Manuscript

NIH-PA Author Manuscript

(Invitrogen) was done simultaneously at a final concentration of 1 μM. Staining was done at 37°C in a 5% CO_2 atmosphere for 15 min, cell suspensions were diluted with chilled buffer, placed on ice and analyzed within 30 min. Flow cytometry demonstrated variable amounts of cell debris which appeared most abundantly after exposure to nanocomposites and UV illumination; for that reason we chose to include the debris data in our final analysis of these samples. A similar approach was used by others in the literature.[30]

Conclusion

DNA binding peptides such as the KH peptide can serve to anchor ROS forming nanocomposites close to DNA which in turn can potentiate inducible DNA damage. Investigation of peptides derived from other DNA interacting proteins such as transcription factors or repair proteins may provide new avenues for fine tuning nanocomposite targeting which should, in turn, increase efficiency of nanocomposite treatments.

Supplementary Material

Refer to Web version on PubMed Central for supplementary material.

Acknowledgments

We would like to acknowledge help from the following core facilities: Cell Imaging Facility, Flow Cytometry Core Facility and Quantitative Bioelemental Imaging Center supported in part by Northwestern University Cancer Center. We also thank Dr. Lou Laimins for the use of pGEMII H18 plasmid. This work was supported by the NIH grants EB002100 and U54 CA151880 and institutional collaboration supporting exchange between NU and University of Alexandria.

Notes and references

1. Bailar JC 3rd, Gornik HL. N Engl J Med. 1997; 336:1569–1574. [PubMed: 9164814]
2. Greish K. Methods Mol Biol. 2010; 624:25–37. [PubMed: 20217587]
3. LaRocque J, Bharali DJ, Mousa SA. Mol Biotechnol. 2009; 42:358–366. [PubMed: 19291428]
4. Talekar M, Kendall J, Denny W, Garg S. Anticancer Drugs. 2011; 22:949–962. [PubMed: 21970851]
5. Wamer WG, Yin JJ, Wei RR. Free Radic Biol Med. 1997; 23:851–858. [PubMed: 9378364]
6. Tachikawa T, Majima T. Chem Soc Rev. 2010; 39:4802–4819. [PubMed: 20824247]
7. Sanders K, Degn LL, Mundy WR, Zucker RM, Dreher K, Zhao B, Roberts JE, Boyes WK. Toxicol Appl Pharmacol. 2012; 258:226–236. [PubMed: 22115978]
8. George S, Pokhrel S, Ji Z, Henderson BL, Xia T, Li L, Zink JI, Nel AE, Madler L. J Am Chem Soc. 2011; 133:11270–11278. [PubMed: 21678906]
9. Rozhkova EA, Ulasov I, Lai B, Dimitrijevic NM, Lesniak MS, Rajh T. Nano Lett. 2009; 9:3337–3342. [PubMed: 19640002]
10. Li SQ, Zhu RR, Zhu H, Xue M, Sun XY, Yao SD, Wang SL. Food Chem Toxicol. 2008; 46:3626–3631. [PubMed: 18840495]
11. Meena R, Rani M, Pal R, Rajamani P. Appl Biochem Biotechnol. 2012; 167:791–808. [PubMed: 22614867]
12. Arora HC, Jensen MP, Yuan Y, Wu A, Vogt S, Paunesku T, Woloschak GE. Cancer Res. 2012; 72:769–778. [PubMed: 22158944]
13. Yao KF, Peng Z, Liao ZH, Chen JJ. J Nanosci Nanotechnol. 2009; 9:1458–1461. [PubMed: 19441546]

NIH-PA Author Manuscript

NIH-PA Author Manuscript

NIH-PA Author Manuscript

14. Thurn KT, Paunesku T, Wu A, Brown EM, Lai B, Vogt S, Maser J, Aslam M, Dravid V, Bergan R, Woloschak GE. Small. 2009; 5:1318–1325. [PubMed: 19242946]
15. Haley B, Paunesku T, Protic M, Woloschak GE. Int J Radiat Biol. 2009; 85:643–655. [PubMed: 19579069]
16. Makeyev AV, Liebhaber SA. RNA. 2002; 8:265–278. [PubMed: 12003487]
17. Baber JL, Libutti D, Levens D, Tjandra N. J Mol Biol. 1999; 289:949–962. [PubMed: 10369774]
18. Vosa L, Sudakov A, Remm M, Ustav M, Kurg R. J Virol. 2012; 86:348–357. [PubMed: 22031941]
19. Schultz LB, Chehab NH, Malikzay A, Halazonetis TD. J Cell Biol. 2000; 151:1381–1390. [PubMed: 11134068]
20. Wyllie AH, Kerr JF, Currie AR. Int Rev Cytol. 1980; 68:251–306. [PubMed: 7014501]
21. Raha S, Paunesku T, Woloschak G. Wiley Interdiscip Rev Nanomed Nanobiotechnol. 2011; 3:269–281. [PubMed: 21046660]
22. Soenen SJ, Himmelreich U, Nuytten N, De Cuyper M. Biomaterials. 2011; 32:195–205. [PubMed: 20863560]
23. Rajh T, Dimitrijevic NM, Rozhkova EA. Methods Mol Biol. 2011; 726:63–75. [PubMed: 21424443]
24. Paunesku T, Rajh T, Wiederrecht G, Maser J, Vogt S, Stojicevic N, Protic M, Lai B, Oryhon J, Thurnauer M, Woloschak G. Nat Mater. 2003; 2:343–346. [PubMed: 12692534]
25. Paunesku T, Vogt S, Lai B, Maser J, Stojicevic N, Thurn KT, Osipo C, Liu H, Legnini D, Wang Z, Lee C, Woloschak GE. Nano Lett. 2007; 7:596–601. [PubMed: 17274661]
26. Thurn KT, Arora H, Paunesku T, Wu A, Brown EM, Doty C, Kremer J, Woloschak G. Nanomedicine. 2011; 7:123–130. [PubMed: 20887814]
27. Karstensen B, Poppelreuther S, Bonin M, Walter M, Iftner T, Stubenrauch F. Virology. 2006; 353:200–209. [PubMed: 16814354]
28. McMahon SJ, Currell FJ. Radiat Res. 2011; 175:797–805. [PubMed: 21466384]
29. Moore GE, Sandberg AA. Cancer. 1964; 17:170–175. [PubMed: 14123677]
30. Minervini F, Fornelli F, Flynn KM. Toxicol In Vitro. 2004; 18:21–28. [PubMed: 14630058]

NIH-PA Author Manuscript

NIH-PA Author Manuscript

NIH-PA Author Manuscript

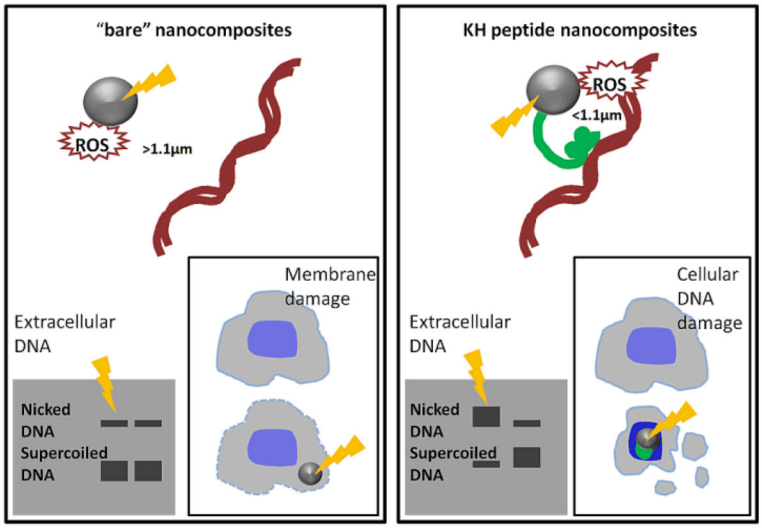

Figure 1.

Schematic representation of experiments performed with the KH-peptide functionalized nanoconjugates.

NIH-PA Author Manuscript

NIH-PA Author Manuscript

NIH-PA Author Manuscript

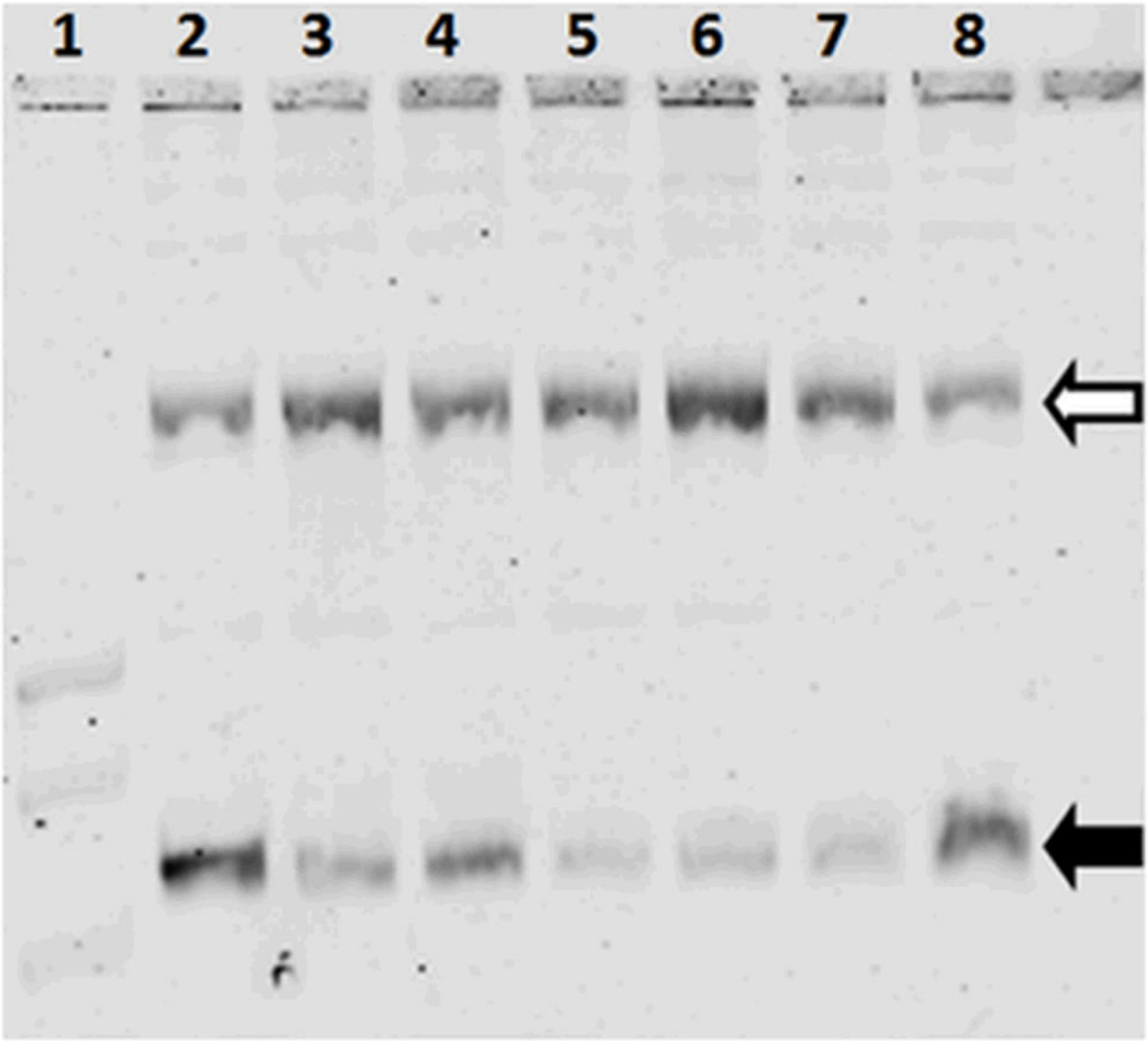

Figure 2.

DNA breakage in the presence of illuminated nanocomposites with differently functionalized surfaces. Lane 1 contains the DNA molecular weight marker; lane 2 is the DNA of the plasmid pGEMII18-WT without addition of any type of nanoparticle. Arrows point to the two forms of DNA: supercoiled DNA indicated by black arrow travels through the gel most rapidly; presence of DNA damaged sites causes plasmid relaxation, this form of DNA, indicated by white arrow, travels through the gel more slowly. Lanes 3 and 4 are pGEMII18-WT plasmid DNA mixed with bare Fe3O4@TiO2 nanoparticles after (3) or before (4) illumination. Lanes 5 and 6 are pGEMII18-WT mixed with Fe3O4@TiO2 nanoparticles covered with ARS only, after or before illumination, respectively. Lanes 7 and 8 are pGEMII18-WT mixed with Fe3O4@TiO2 nanoparticles coated with both KH peptide and Alizarin red S, after (7) or before (8) illumination.

NIH-PA Author Manuscript

NIH-PA Author Manuscript

NIH-PA Author Manuscript

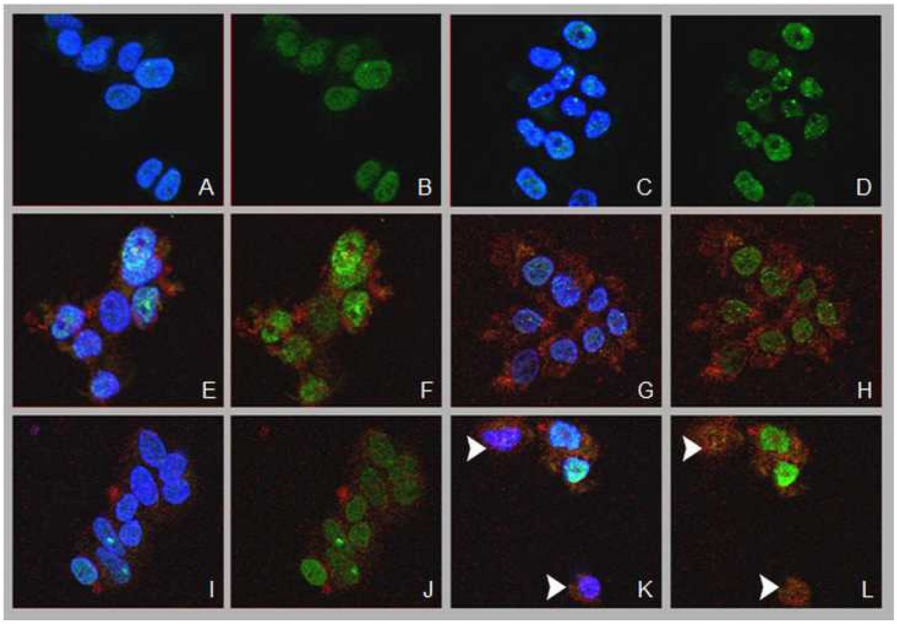

Figure 3.

Confocal microscopy images of RPMI 2650 cells treated with nanocomposites and illuminated to activate production of ROS: A, B) control cells in the absence of UV exposure. In control cells 53BP1 is homogenously distributed within the nucleus of the cells, with a solitary focus in some of the cells. C,D) Exposure of control cells to UV light slightly increases the number of 53BP1 foci. E,F) cells treated with ARS covered nanoparticles in the absence of UV exposure, 53BP1 is diffusely distributed within the nucleus without evident nuclear changes. G,H) Cells incubated with non-targeted nanoparticles, covered with ARS only, and exposed to UV light show some 53BP1 foci. I,J) Cells incubated with nanocomposites conjugated to ARS and functionalized with KH-peptide display cytoplasmic as well as nuclear distribution of the nanoparticles. In absence of exposure to a UV light, 53BP1 is homogenously distributed within the nucleus. K,L) UV illumination of cells treated with nanoparticles coated with ARS and KH-peptide lead to development of foci in some of the cells although some cells present only deeply stained small nuclei and shrunken cytoplasm and no staining for 53BP1 (Arrows). (A, C) blue Hoechst staining for DNA and green staining for 53BP1; (B, D) green staining for 53BP1 only; (E, G, I, K) blue Hoechst staining for DNA, green staining for 53BP1 and red staining (ARS) for nanoparticles; (F, H, J, L) green staining for 53BP1 and red staining (ARS) for nanoparticles.

NIH-PA Author Manuscript

NIH-PA Author Manuscript

NIH-PA Author Manuscript

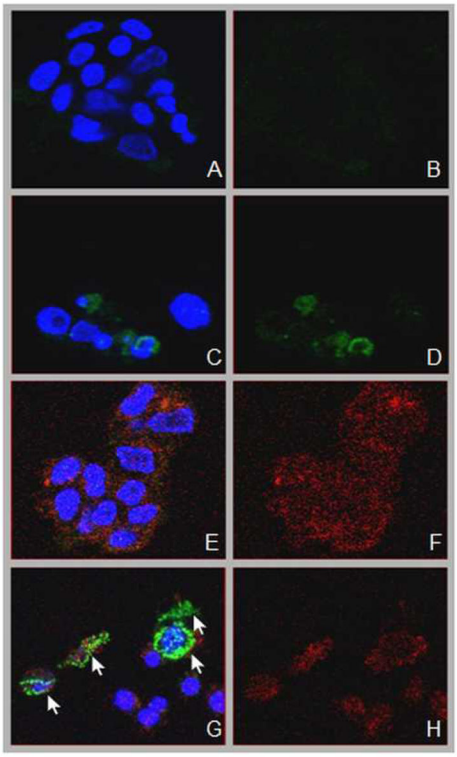

Figure 4.

Confocal microscopy of RPMI 2640 cells for detection of apoptosis under the following conditions: A, B) control, untreated cells (; C,D) control cells following exposure to UV light; E, F) cells treated with nanocomposites coated with ARS and functionalized by KH peptide, without exposure to UV light;; G,H) Cells incubated with KH-peptide functionalized nanocomposites and exposed to ultraviolet light show occasional M30 staining (Arrows). (A, C) blue Hoechst staining of DNA; (B, D) green staining with M30 only; (E, G) blue Hoechst staining of DNA; green staining for M30 and red staining for nanoparticles; (F, H) red staining for nanoparticles only.

NIH-PA Author Manuscript

NIH-PA Author Manuscript

NIH-PA Author Manuscript

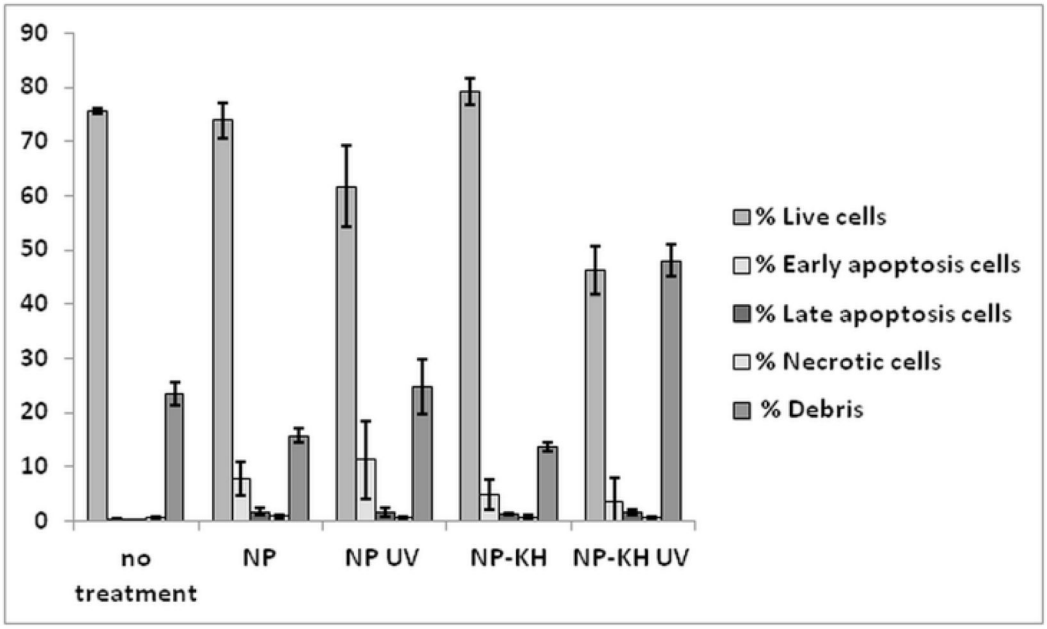

Figure 5.

Flow cytometric analysis of nanocomposite treated cells with or without light activation. Cell staining was done with annexin V (apoptosis positive cells) and SYTOX-blue (necrotic cells). In addition, cellular debris was quantified on the basis of side scatter.